공학석사 학위논문

Solvothermal Synthesis of Molybdenum Disulfide/Reduced Porous Graphene Oxide Nanocomposite as High Performance Anode Material for Lithium Ion Battery

용매열 합성을 통한 이황화 몰리브덴/환원 다공성 그래핀 옥사이드 나노 복합체의 합성 및 리튬 이온 배터리용 음극재 활용

2017년 2월

서울대학교 융합과학기술대학원

융합과학부 나노융합전공

배 영 국

Solvothermal Synthesis of Molybdenum Disulfide/ Reduced Porous Graphene Oxide Nanocomposite as High Performance Anode Material for Lithium Ion Battery

용매열 합성을 통한 이황화 몰리브덴/ 환원 다공성 그래핀 옥사이드 나노 복합체의 합성 및 리튬 이온 배터리용 음극재 활용

지도 교수 박 원 철

이 논문을 공학석사 학위 논문으로 제출함

2017 년 1 월

서울대학교 융합과학기술대학원

융합과학부 나노융합전공

배 영 국

배영국의 공학석사 학위논문을 인준함

2017 년 2 월

위 원 장 김 연 상 (인)

부 위 원장 박 원 철 (인)

위 원 송 윤 규 (인)

Abstract

Solvothermal Synthesis of Molybdenum Disulfide/Reduced Porous Graphene Oxide Nanocomposite as High Performance Anode Material for Lithium Ion Battery

Youngkuk Bae

Program in Nano Science and Technology

Graduate School of Convergence Science and Technology

Seoul National University

Lithium ion batteries are widely used as power sources for portable electronic devices and hybrid electric vehicles. Electrode materials with high lithium storage capacity have been studied to meet the requirements of these applications. Among these materials, molybdenum disulfide (MoS_2) is one of promising anode material to replace commercial graphite anode because intercalation of a MoS_2

with 4 Li^+ ions results in a higher storage capacity for MoS_2 (670 mA h g^{-1}) than commercial graphite anodes (372 mA h g^{-1}). Although MoS_2 has a high theoretical capacity than graphite as an anode material for Lithium-ion battery, its intrinsic poor electrical/ionic conductivity decreases rate property and lithium storage capacity. In my thesis, I prepared MoS_2/reduced porous graphene oxide (rPGO) composite by solvothermal method to complement conductivity and improve lithium storage properties of MoS_2. PGO was synthesized by convenient, low-cost, and mass-producible nitric acid treatment method. Due to its enlarged surface area and porous structure, MoS_2/rPGO sample exhibited improved capacity and cyclic stability than other MoS2/reduced graphene oxide (rGO) and MoS_2 nanoparticle samples. After 100 cycles, MoS_2/rPGO electrode shows improved capacity of 932 mA h g^{-1} while capacity of MoS_2/rGO electrode is 395 mA h g^{-1} at 200 mA g^{-1}.

keywords: Lithium ion battery, anode, porous graphene oxide, molybdenum disulfide, carbon composite

Student Number: 2015-26026

Contents

Abstract ……...i

Contents ……..iii

List of Figure ...……..v

1. Introduction

1.1 Lithium-ion battery ……..…….1

1.2 Molybdenum disulfide ……...3

1.3 Porous graphene oxide ……...3

2. Experimental

2.1 Materials ……..5

2.2 Synthesis of graphene oxides ……..5

2.3 Synthesis of porous graphene oxides ……..5

2.4 Solvothermal synthesis of Molydenum disulfide/reduced porous graphene oxide nanocomposite ……6

2.5 Structural and morphological characterization ……6

2.6 Electrochemical characterization ……7

3. Result and Discussion

3.1 Structural and morphological characterization ……9

3.2 Electrochemical characterization ……19

4. Conclusion ……27

References ……28

국 문 초 록 ……..34

List of Figures

Figure 1 Molecular models of (a) 2H–MoS_2. (b) Lithiated 2H–MoS_2 showing a 5% lattice expansion in the c-direction and a-direction due to intercalation. (c) Lithiated 1T–MoS_2 showing lithium ions occupying octahedral interstices. (d) 3R–MoS_2 (e) Li_2S …… - 2 -

Figure 2 Schematic illustration of the MoS_2/rPGO composite synthesis - 8 -

Figure 3 SEM images of (a) MoS_2/rGO, (b) MoS_2/rPGO; TEM images of (c) MoS_2/rGO, (d) MoS_2/rPGO; HRTEM images of (e) MoS_2/rGO, (f) MoS_2/rPGO. …… - 10 -

Figure 4 (a) XRD patterns of MoS_2/rGO and MoS_2/rPGO; (b) TGA curves of MoS_2 nanoparticle, MoS_2/rGO and MoS_2/rPGO. ……. - 11 -

Figure 5 (a) XPS survey scan and spectra of (b) Mo 3d, (c) S 2p and (d) C 1s for MoS_2/rPGO. …… - 13 -

Figure 6 (a) XPS survey scan and spectra of (b) Mo 3d, (c) S 2p and (d) C 1s for MoS_2/rGO. ……..…. - 14 -

Figure 7 (a) Nitrogen adsorption-desorption isotherms at 77 K and (b) pore-width distribution of MoS_2/rGO and MoS_2/rPGO composites. …… - 16 -

Figure 8 (a) Nitrogen adsorption-desorption isotherms at 77 K and (b) pore-width distribution of rGO and rPGO composites. …… - 17 -

Figure 9. Raman spectra of rGO and rPGO in samples. ……. - 18 -

Figure 10 CVs of (a) MoS_2 nanoparticles, (b) MoS_2/rGO and (c) MoS_2/rPGO electrode for first to third cycles at a scan rate of 0.5 mV s^{-1}. First charge/ discharge profiles of (d) MoS_2 nanoparticles and (e) MoS_2/rGO and (f) MoS_2/ rPGO electrode at a current density of 200 mA g^{-1}. …… - 21 -

Figure 11 Nyquist plots of MoS_2/rGO and MoS_2/rPGO, before and after 5 cycles at 1 A g^{-1}. …….. - 22 -

Figure 12 (a) Cycling performance at a current density of 200 mAg^{-1} and (b) rate capability performance of MoS_2 nanoparticles, MoS_2/rGO, MoS_2/rPGO. .....- 24 -

Figure 13 Rate capability performance of MoS_2/rPGO composite, a) synthesized using 12M, 8M and 4M nitric acid treat PGO as a substrate and b) synthesized using 130, 150 and 170g of $(NH_4)_2MoS_4$ as a precursor. - 27 -

1. Introduction

1.1 Lithium-ion battery

The need for electrical energy storage increases with time as a result of change in lifestyle and economic growth. Many applications such as portable electronics and electric vehicles rely on electrical energy storage. But as energy consumption increases, worries about environmental pollution and exhaustion of resource are becoming serious. Due to these concerns, alternative energy sources such as solar, wind and wave energy need to be developed. However, these renewable resources need energy storage devices because these energy is intermittent. Therefore, it is important to improve performance of energy storage for expansion of energy based on renewable sources.[1]

Energy storage systems with high energy and power density are demanded to store energy from renewable sources. Among the electrochemical energy storage devices, rechargeable batteries are one of the most promising options. Various rechargeable battery systems have used for over a century in a many applications. But as the portable electronics become smaller, advanced rechargeable batteries have to be developed. Energy density, power, cost and safety are important requirement of batteries.[2]

Lithium-ion batteries (LIBs) are widely used as power sources for portable electronic devices due to their high energy capacity and relatively long lifespan.[3] The market demand for higher performance has led to many materials, such as silicon,[4] transition metal oxide[5, 6] and sulfide,[7] being extensively studied for use as alternative anode materials in LIBs due to their higher lithium storage capacity.

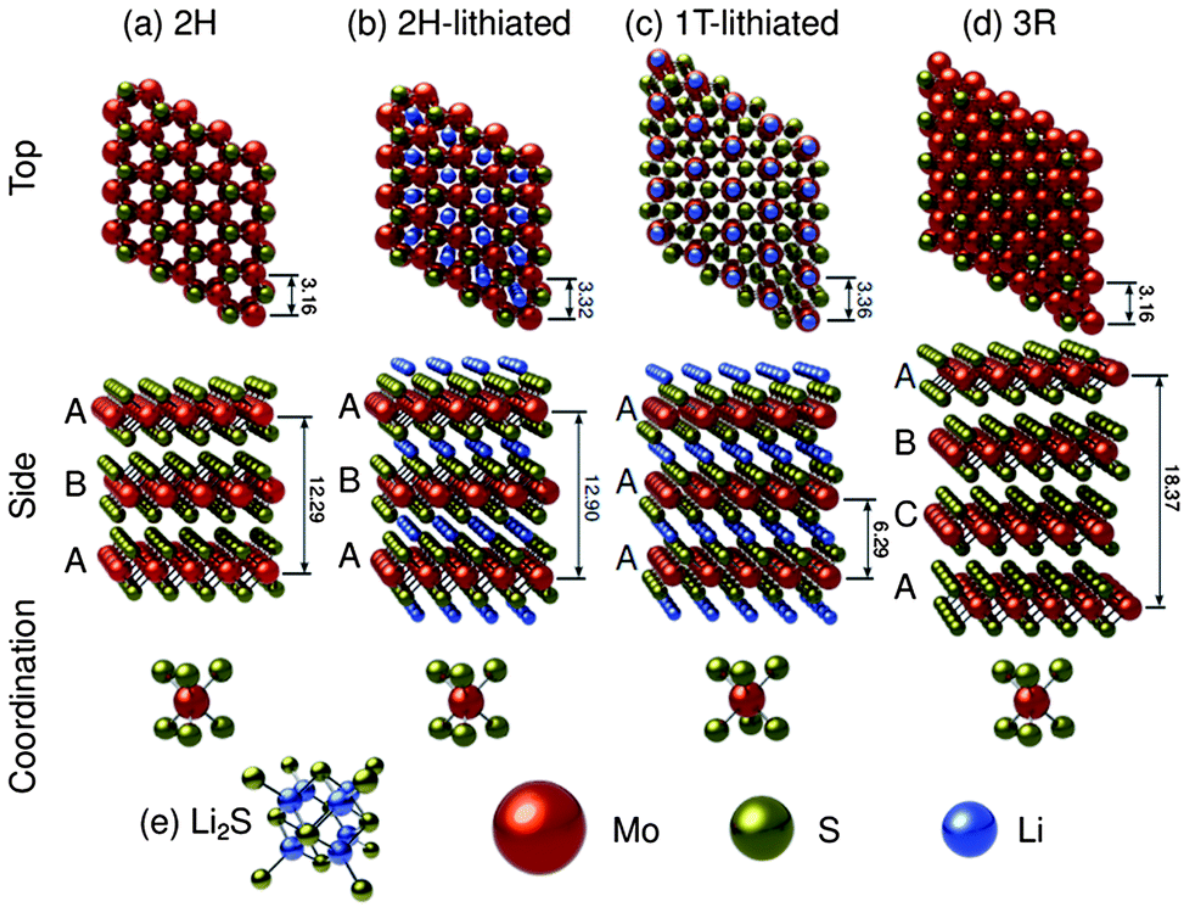

Figure 1 Molecular models of (a) 2H–MoS_2. (b) Lithiated 2H–MoS_2 showing a 5% lattice expansion in the c-direction and a-direction due to intercalation. (c) Lithiated 1T–MoS_2 showing lithium ions occupying octahedral interstices. (d) 3R–MoS_2 (e) Li_2S (domains of this phase would be interspersed with molybdenum nanoparticles). Dimensions are shown in Angstroms. Adapted from ref. 11 (DOI: 10.1039/C3EE42591F) with permission.

1.2 Molybdenum disulfide

Among these materials, molybdenum disulfide (MoS_2) has drawn attention as a promising anode material. MoS_2 is a layered material analogous to graphite wherein the Mo and S atoms in each layer are bound by strong covalent bonds and the layers are stacked by weak van der Waals forces.[8] Three main structures of MoS_2 depicted in Figure 1 are 2H-MoS_2, 3R-MoS_2 and 1T-MoS_2. Intercalation of a MoS_2 with 4 Li^+ ions results in a higher storage capacity for MoS_2 (670 mA h g^{-1}) than commercial graphite anodes (372 mA h g^{-1}); a lower cycle fading than other active materials such as Si or Ge makes MoS_2 a good candidate for an anode material in LIBs.[9-11] The low electrical/ionic conductivity of MoS_2 itself results in poor cycle performance and low rate capability.[12] Volume expansion and pulverization are other major drawbacks that impede the electrochemical properties of the MoS_2 anode.[13]

Nanostructure modification[14] or hybridization with a conducting material[15-18] have been studied and shown to be successful methods to overcome these problems.[19] Graphene,[20-22] carbon nanotubes[23, 24] and conductive polymers[25] composited with MoS2 have been studied in this context. Among them, graphene has been considered as the most desirable matrix owing to its good electrical conductivity, high surface area and thermal/chemical stability.[18, 26] With these attempts, the resulting MoS_2 nano-composites show improved electrochemical properties because of the buffering of the volume expansion during cycling and by supplementing conductivity of MoS_2.[27, 28]

1.3 Porous graphene oxide

To overcome these problems, nanostructure modification[14] or hybridization with a conducting material[15-18] have been studied and proven to be successful methods.[19] Typically, graphene,[20, 21] CNT[23, 24] and conductive polymers[25] composited with MoS_2 were studied in this context. Among them, graphene has been considered as the most desirable matrix owing to its good electrical

conductivity, high surface area and thermal/chemical stability.[18, 26] With those attempts, the resulting MoS_2 nanocomposites show improved electrochemical properties not only because of the buffering the volume expansion during cycling but also supplementing conductivity of MoS_2.[27, 28]

In recent years, porous graphene and its compounds have been developed as anode materials with further improved electrochemical properties due to their unique porous structure combined with inherent properties of graphene.[29] Porous structure provides ion diffusion channel facilitating not only Li ion storage but also transport at high rate current densities.[30, 31] Moreover, these porous materials exhibited enhanced cycling stability during lithiation/delithiation cycles due to unique structure preventing agglomeration between sheets.[32-35] Preparation of porous graphene can be roughly categorized into out-of-plane producing of 3D porous structure and in-plane creation of defective pores into sheets. 3D out-of-plane porous graphene can be built up by template[36, 37] or hydrothermal methods[38] while in-plane porous graphene can be synthesized by carbon erosion under acid/oxidizer solution. Among attempts to produce in-plane porous graphene, Shi *et al*. recently reported a one-step porous graphene oxide preparation by refluxing GO sheets in nitric acid solution, which is a robust and easy scalable method.[39] Until now, 3D out-of-plane porous graphene/MoS_2 composites have been studied as anode materials for LIBs.[40-42] However, to the best of our knowledge, in-plane porous graphene/MoS_2 composite as an anode material has not been studied yet.

Here, I report about synthesis of in-plane porous graphene/MoS_2 composite (MoS_2/rPGO) via solvothermal method. PGO powder was prepared by nitric acid treatment and ammonium tetrathiomolybdate were used as a precursor for MoS_2 growth. Brunauer–Emmett–Teller method was conducted to analyze sample's porosity and surface area and morphology of composites was identified using scanning electron microscopy. MoS_2/rPGO composite exhibited lager surface area and pore volume than MoS_2/rGO composite while they show no significant morphology difference. As a result, MoS_2/rPGO composite exhibits high capacity, good cycling retention (932 mA h g^{-1} at 200 mA g^{-1} after 100 cycles) and improved rape capability (451 mA h g^{-1} at 2 A g^{-1}) as anode material for Lithium-ion battery.

2. Experimental

2.1 Materials

Graphite powder (<20 micron, synthetic), phosphorus pentoxide (P2O5, 97 %), potassium permanganate (KMnO4, 99.3 %), potassium persulfate ($K_2S_2O_8$), sulfuric acid (H_2SO_4, 95-98 %), ammonium thiomolybdate {$(NH_4)_2MoS_4$)}, N,N-dimethylformamide (DMF) and hydrazine (N_2H_4) from Aldrich and nitric acid (HNO_3, 68~70%) and hydrochloric acid (HCl, 35.0-37.0 %) from SAMCHUN were purchased, respectively. All reagents were used without further purification.

2.2 Synthesis of graphene oxides

Graphene oxide (GO) was synthesized from graphite powder (<20 micron) by a modified Hummers methods.[43] Briefly, 3 g of graphite, phosphorus pentoxide (P_2O_5, 2.5 g) and potassium persulfate ($K_2S_2O_8$, 2.5 g) were dissolved in sulfuric acid (80 ml). The solution was stirred and heated at 95 ℃ for 5 hours. Then it was neutralized using DI water and freeze-dried overnight. The obtained powders were further oxidized by 120 ml of sulfuric acid while 15 mg of $KMnO_4$ were slowly added in ice-bath. This mixture was reacted for another 4 hours at 70 ℃ and then hydrogen peroxide (H_2O_2, 30 wt%) was added. The solution was washed with 1: 10 HCl aqueous solution followed by DI water washings to remove impurities and neutralize. Lastly, the precipitate was freeze-dried.

2.3 Synthesis of porous graphene oxides

Porous graphene oxide (PGO) was prepared by nitric acid treatment method reported by Shi groups.[39] Typically, 250 mg of GO was dissolved in 250 ml 8 M nitric acid solution and refluxed at 100 ℃ for 1 hour. The mixture was washed several times with DI water to neutralize, and then it was freeze-dried.

2.4 Solvothermal synthesis of Molydenum disulfide/reduced porous graphene oxide nanocomposite

The MoS_2/rGO, MoS_2/rPGO nanocomposite and MoS_2 nanoparticle were synthesized by a solvothermal method.[44] To synthesize MoS_2/rPGO sample, 110 mg of ammonium thiomolybdate $\{(NH_4)_2MoS_4\}$ and 150 mg of PGO powder were dissolved in 50 ml N,N-dimethylformamide (DMF) with and 500 µl hydrazine (N_2H_4) and sonicated for 30 min. Then the mixture was transferred into teflon-lined stainless steel autoclave and reacted at 200 ℃ for 10 h. After the solution cooled down to room temperature, the product was washed with DI water and ethanol. To remove other impurities, it was mixed with 3 M HCl solution and stirred. After 1 h of stirring, solution was washed using DI water until neutralized then dried overnight at 80 ℃. MoS_2/rGO sample were obtained using 110 mg GO powder and $(NH_4)_2MoS_4$ each while MoS_2 nanoparticle sample were synthesized with 110 mg of $(NH_4)_2MoS_4$ only.

2.5 Structural and morphological characterization

The Morphology of the composites was characterized by field emission scanning electron microscopy (FE-SEM, Hitachi S-4800), High-resolution transmission electron microscope (TEM) equipped with an energy-dispersive X-ray spectrometer (EDX). X-ray photoelectron spectroscopy (XPS) data were obtained by AXIS-His spectrometer (KRATOS) with a monochromatic Al Ka source. X-Ray diffraction (XRD) patterns were acquired using a New D8-advance, equipped with a Cu Kα source (λ = 1.5406 Å), operating at 40 kV and 40 mA, and using a scan range of 10 º~80 º. Brunauer–Emmett–Teller (BET) method was used to calculate specific surface area. Pore volume and average pore diameter were calculated by Barrett–Joyner–Halenda (BJH) method. Thermogravimetric analysis (TGA) measurement data were acquired by TGA/DSC 1 (Mettler Toledo) analyzer with a

heating rate of 10 ℃ min^{-1} up to 700 ℃ in air. Raman spectra was obtained on a Horiba jobin yvon T64000 Raman Spectrometer equipped with excitation lasers with wavelengths of 514 nm.

2.6 Electrochemical characterization

The working electrode was fabricated by mixing 80 wt% of active material (samples), 10 wt% of binder (PVDF) and 10 wt% of conductive carbon (Super P). These materials were mixed with the n-methyl-2-pyrrolidinone and coated onto the Cu foil by a doctor blade. After drying at 60 ℃ in a vacuum oven for 2 h, the coated foil was compressed and cut into circular electrodes. Electrodes were dried for 12 h in 120 ℃ vacuum oven and transferred to argon-filled glove box. Electrochemical tests were conducted using coin-type half cells (2016 type) assembled in an argon-filled glove box. Lithium metal was used as counter and reference electrodes and the electrolyte was 1.0 M $LiPF_6$ in a mixture of ethylene carbonate/diethyl carbonate (volume ratio 1:1). WBCS3000 cycler system (Wonatech, Korea) was used for galvanostatic charge/discharge (voltage range between 0.01 and 3.0 V vs. Li/Li^+) and cyclic voltammetry (CV) test (scanning rate of 0.5 mV s^{-1}). Electrochemical impedance spectroscopy (EIS) was conducted in the range of 100 kHz to 10 mHz with an AC amplitude of 5 mV on CHI 660e model.

3. Result and Discussion

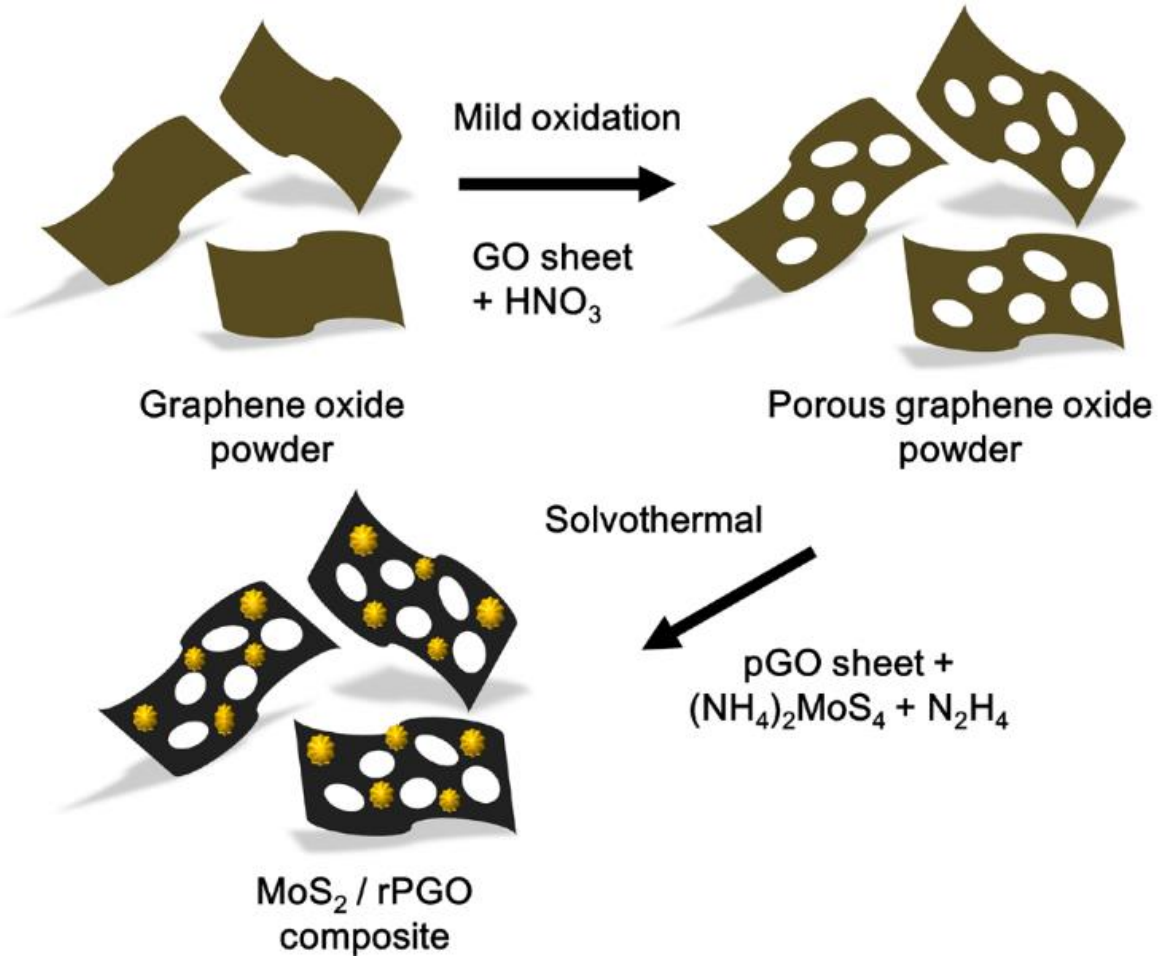

Figure 2 Schematic illustration of the MoS_2/rPGO composite synthesis

3.1 Structural and morphological characterization

The MoS_2/rPGO nanocomposite was synthesized by the solvothermal method depicted in Figure 2. PGO powder was synthesized via nitric acid treatment and $(NH_4)_2MoS_4$ precursor were dissolved in *N*,*N*-dimethylformamide (DMF) with N_2H_4. By solvothermal process, PGO was reduced (rPGO) and the $(NH_4)_2MoS_4$ precursor was decomposed to MoS_2 on the rPGO sheets.[44]

The Morphological images of MoS_2/rGO and MoS_2/rPGO nanocomposites in Figure 3 were obtained by SEM and transmission electron microscope (TEM). Figure 3a&b show that the two nanocomposites exhibit analogous morphologies; the MoS_2 nanoparticles grew on GO and PGO sheets in sphere shapes consisting of disordered MoS_2 nanosheets. Figure 3c-f are TEM and high-resolution transmission electron microscope (HR-TEM) images of MoS_2/rGO and MoS_2/rPGO nanocomposite. In agreement with SEM images, Figure 3c&d show similar growth of MoS_2 nanoparticles on both GO and PGO sheets. MoS_2 interlayer distances of the samples exhibited in Figure 3e&f are larger (~ 0.8 nm) than normal (002) plane interlayer distance of MoS_2 (0.62 nm) due to randomly oriented layers,[45] which corresponds with X-Ray diffraction (XRD) patterns in Figure 4a. [46]

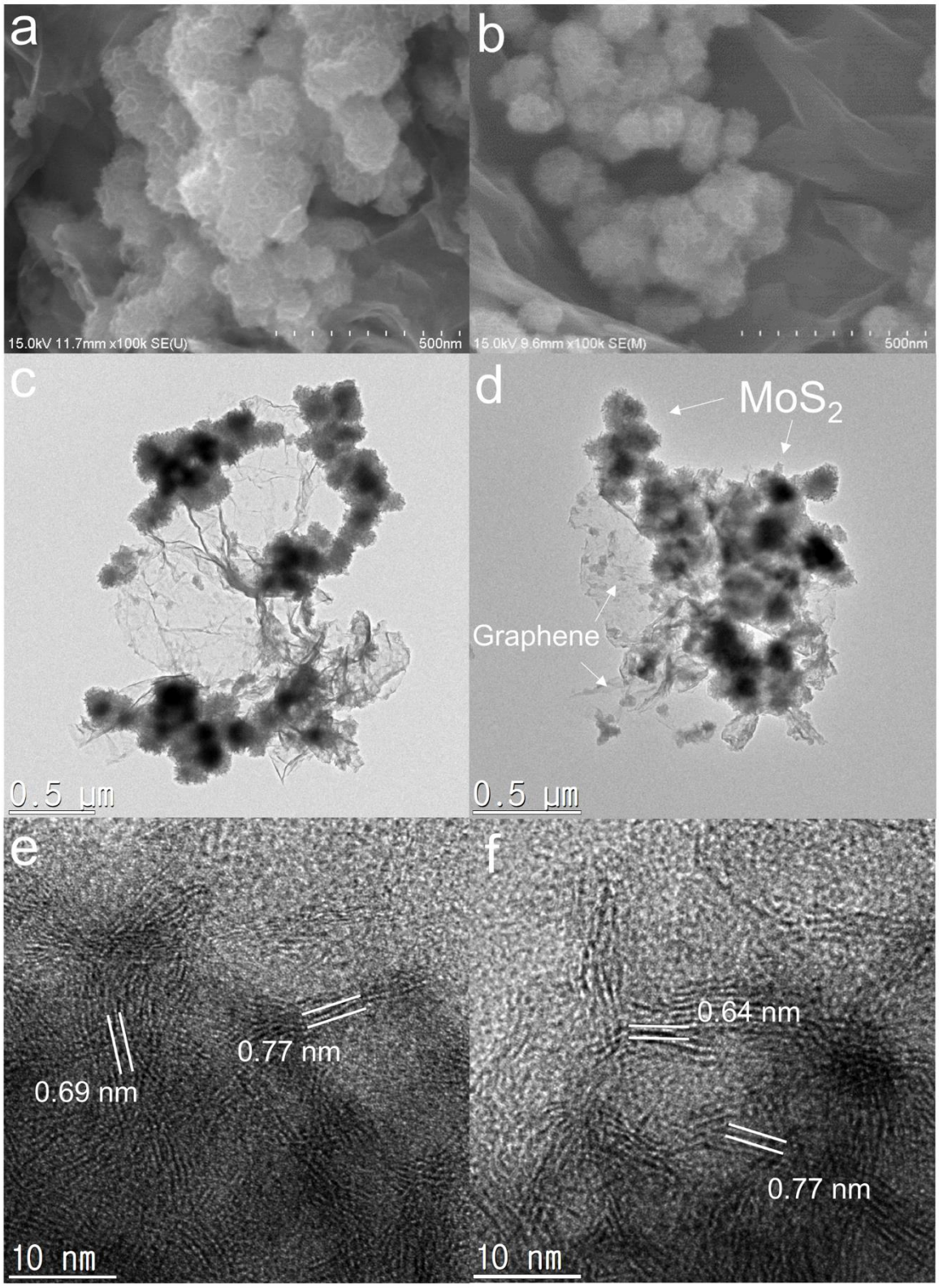

Figure 3 SEM images of (a) MoS_2/rGO, (b) MoS_2/rPGO; TEM images of (c) MoS_2/rGO, (d) MoS_2/rPGO; HRTEM images of (e) MoS_2/rGO, (f) MoS_2/rPGO.

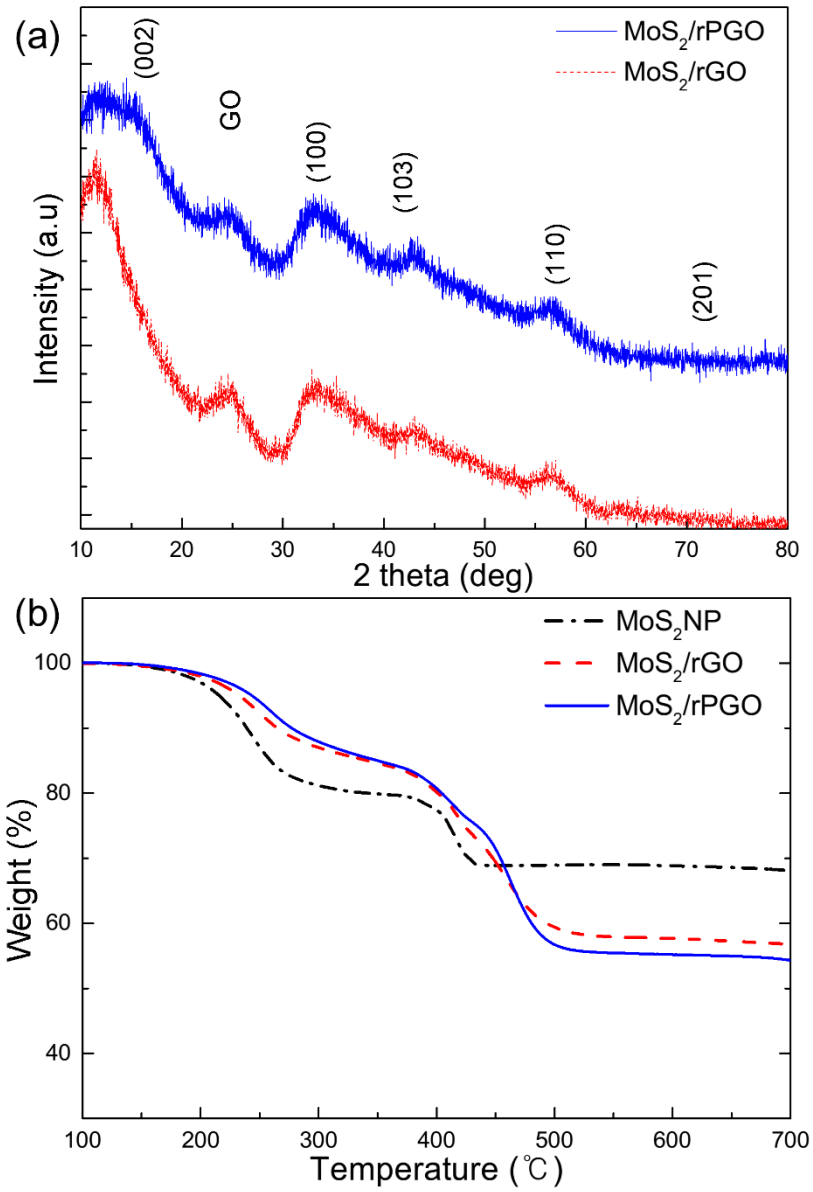

Figure 4 (a) XRD patterns of MoS_2/rGO and MoS_2/rPGO; (b) TGA curves of MoS_2 nanoparticle, MoS_2/rGO and MoS2/rPGO.

Figure 4a shows the XRD patterns of the as-prepared MoS_2/rGO and MoS_2/rPGO nanocomposites. The diffraction peaks of samples can be assigned to (002) peak of rGO, broadened (100), (006) and (110) planes of MoS_2 (JCDPS 37-1492). These broad peaks indicate poor crystallinity of the MoS_2 nano-particles. The peak corres-ponding to the (002) plane of MoS_2 also cannot be found clearly, which suggests that MoS_2 has randomly oriented layers.[45, 47] Figure 4b displays the results of thermogravimetric analysis (TGA) measurements conducted to measure content of graphene in the composites. TGA data were obtained over a range of temperatures from room temperature to 700 ℃. The MoS_2 nanoparticle samples show a weight loss of about 30% at 200~400 ℃ during the oxidation of MoS_2 to MoO_3.[48] MoS_2/rGO and MoS_2/rPGO nanocomposite samples exhibit further weight loss (~10 wt% more) caused by the thermal decomposition of liable oxygen functional groups of rGO and rPGO.[49, 50]

X-ray photoelectron spectroscopy (XPS) was conducted to verify the existence of MoS_2 and rGO in composite. The XPS survey scan (Figure 5a) of MoS_2/rPGO shows signals for sulfur, molybdenum, carbon and oxygen. The binding energies of Mo 3d 5/2 (228.7 eV), Mo 3d 3/2 (232.2 eV), S 2p 3/2 (161.7 eV) and S 2p 1/2 (163.1 eV) exhibit the dominance of Mo^{4+} and S^{2-}. Oxygen peaks and oxidized molybdenum forms (MoO_3 and MoS_4^{2-}) are derived from oxygen of GO and PGO. Figure 5d indicates remnant C-O bonds (285.7 eV) and carbonyl groups (288.3 eV) after the solvothermal process. XPS peaks of MoS_2/rGO nanocomposite in Figure 6 are similar to the peaks of MoS_2/rPGO sample.

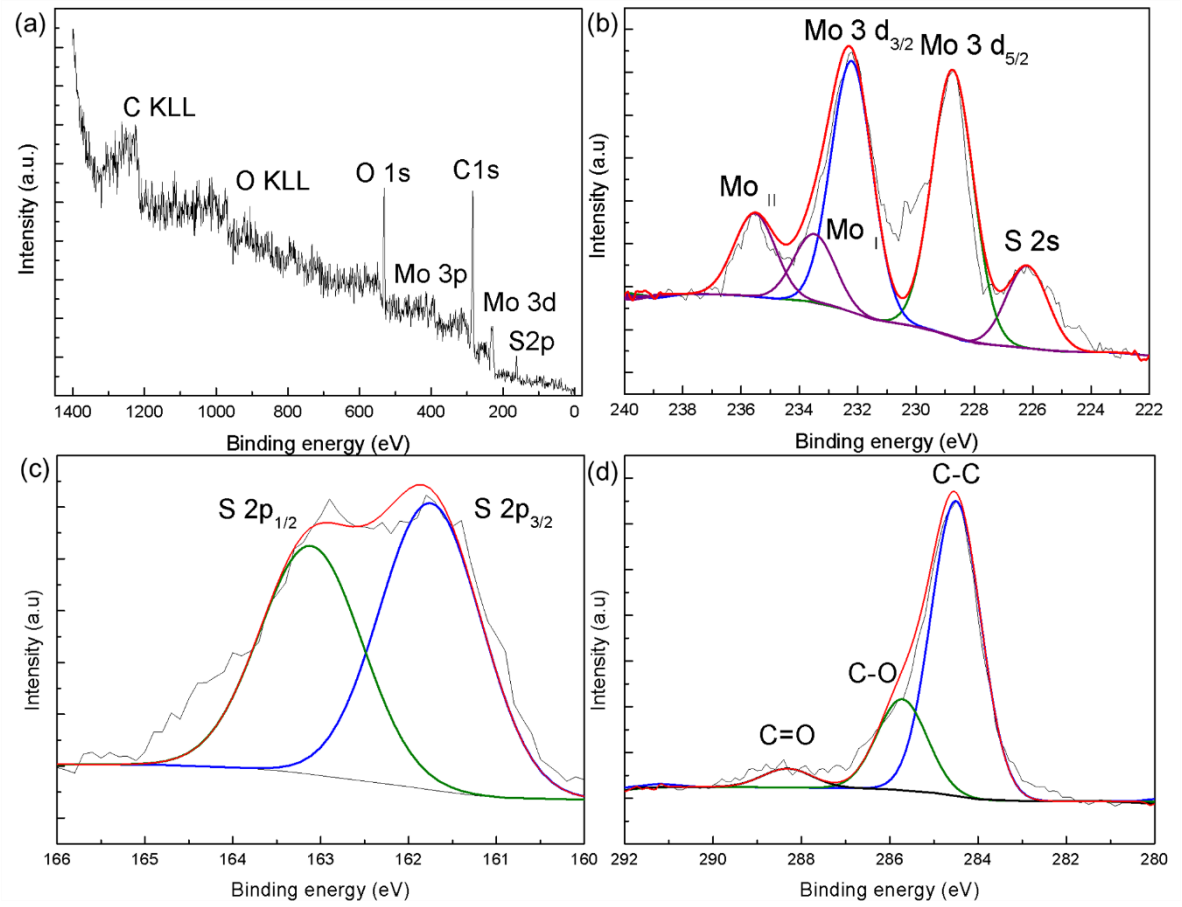

Figure 5 (a) XPS survey scan and spectra of (b) Mo 3d, (c) S 2p and (d) C 1s for MoS_2/rPGO.

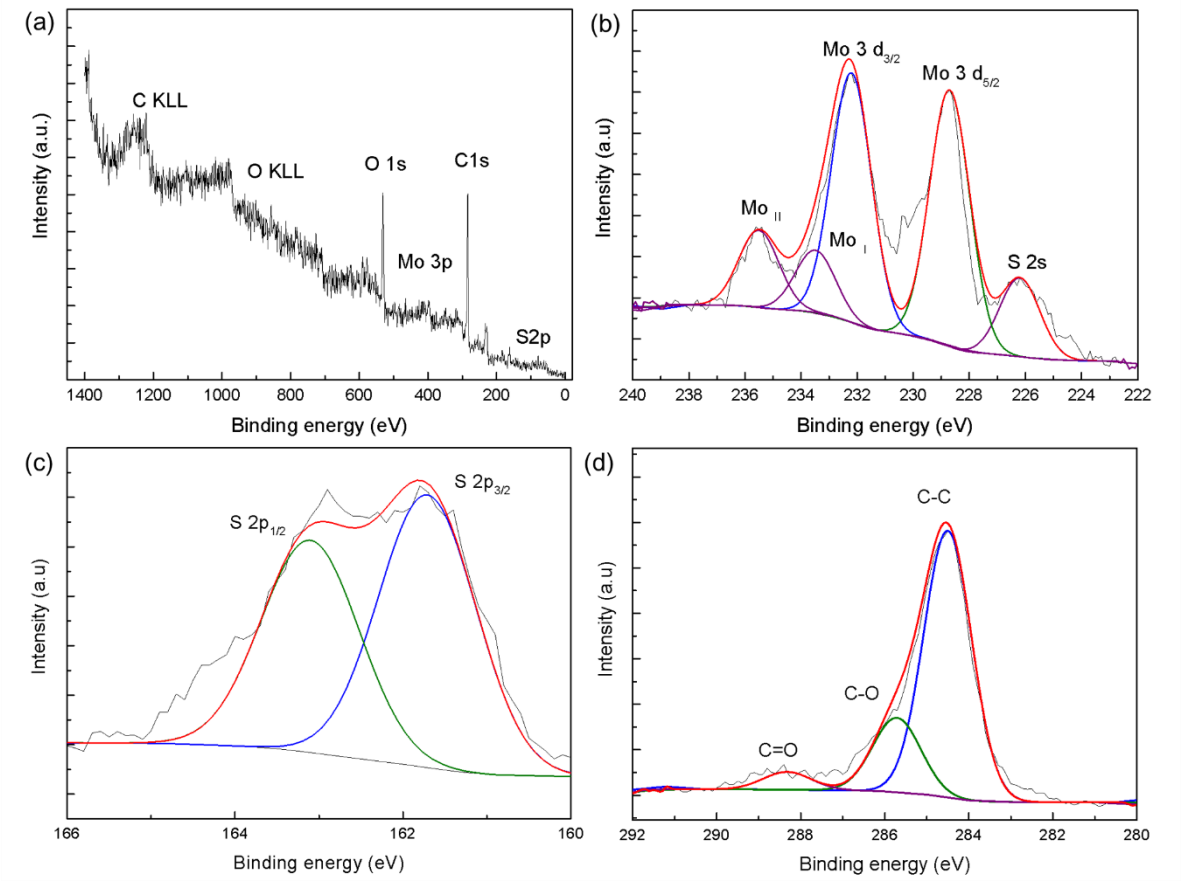

Figure 5 (a) XPS survey scan and spectra of (b) Mo 3d, (c) S 2p and (d) C 1s for MoS_2/rGO.

BET and Barrett–Joyner–Halenda (BJH) analysis were conducted to measure surface areas and pore volumes of MoS_2/rGO and MoS_2/rPGO nanocomposites. In Figure 7a, MoS_2/rGO sample shows type Ⅳ isotherms with higher nitrogen absorption indicating the enlarged surface area and pore volume than the MoS_2/rGO sample. The BJH analysis indicated an increased pore distribution and volume (Figure 7b). The Surface area of MoS_2/rPGO was measured to be 92.26 $m^2\ g^{-1}$ (MoS_2/rGO: 59.20 m^2g^{-1}) and its pore volume was 0.40 cm^2g^{-1} (MoS_2/rGO: 0.26 cm^3g^{-1}). This increse in the surface area and the pore volume could be attributed to porous structure of rPGO.[39] Bare rPGO powder also show a larger surface area and pore volume (148.26 $m^2\ g^{-1}$, 0.53 $cm^3\ g^{-1}$) than that of rGO powder (109.09 $m^2\ g^{-1}$, 0.34 $cm^3\ g^{-1}$) depicted in Figure 8.

Raman spectrocopy was used to charicterize structural change between rGO and rPGO of samples. In Figure 9, both sample shows similar peaks excpet slight difference in relative intensity of D and G bands *(I_D/I_G)*. Samples show two Raman bands, D and G band, at around 1350 and 1594 cm^{-1}. The relative intensity of two Raman band is associated with defect concentration of graphene oixde. D band is related to defects such as vacancies and other amorphous carbon species while G band is associated with sp^2-bonded carbon atoms.[51] So, Increase in I_D/I_G ratio of rPGO/MoS_2 indicates rPGO possess more pores owing to existence of defects.[52]

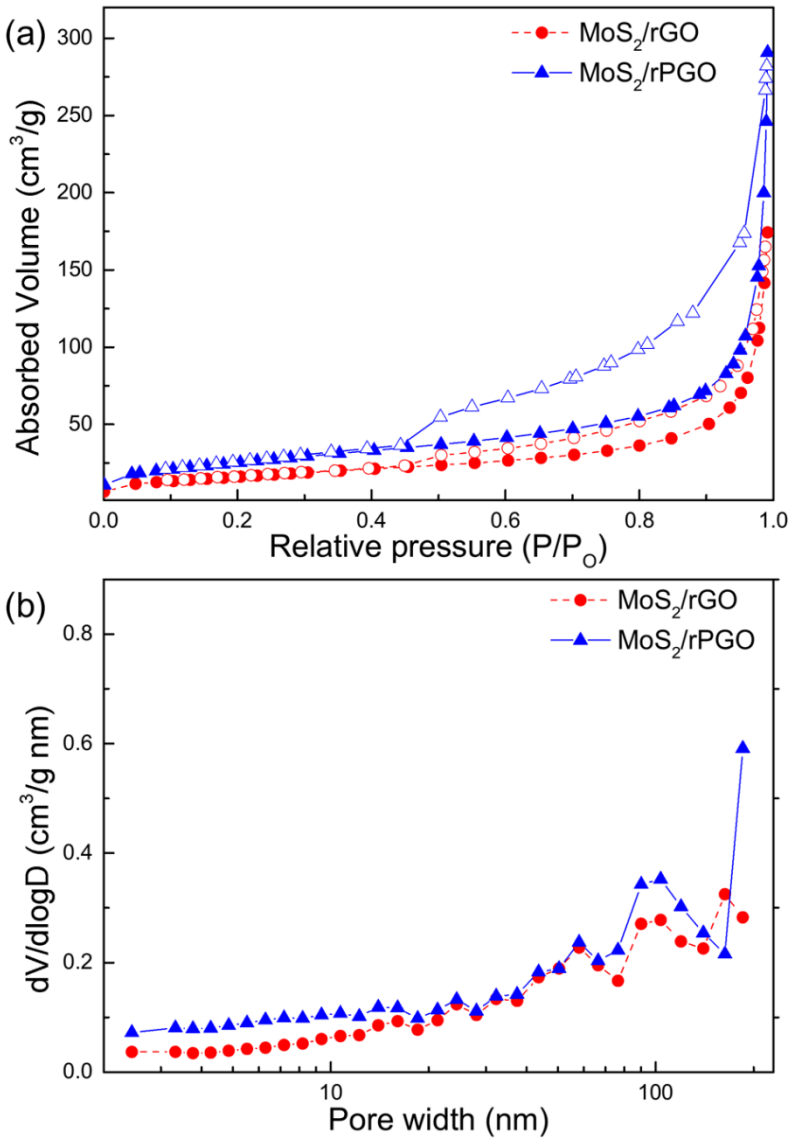

Figure 7 (a) Nitrogen adsorption-desorption isotherms at 77 K and (b) pore-width distribution of MoS_2/rGO and MoS_2/rPGO composites.

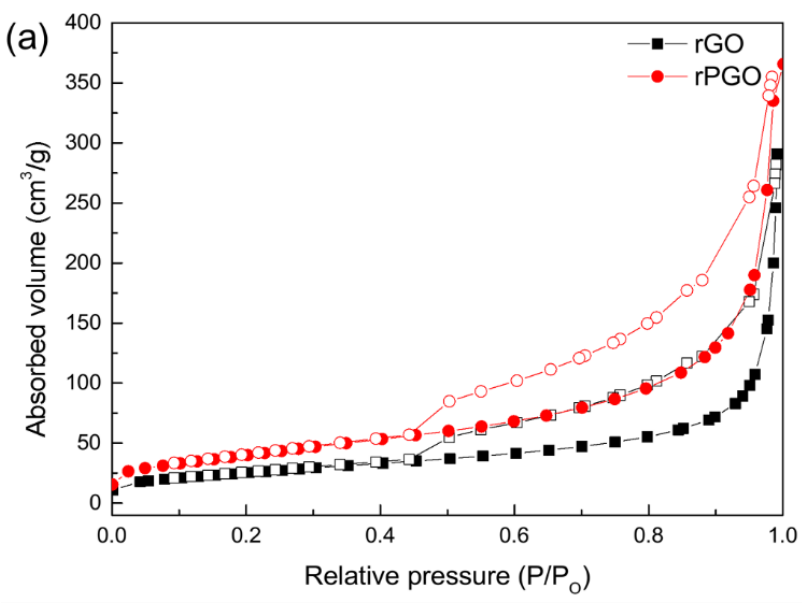

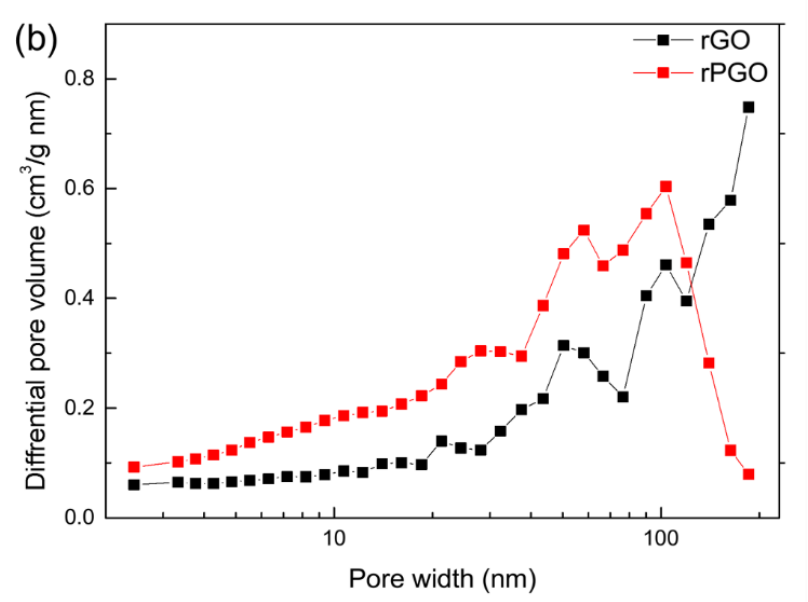

Figure 8 (a) Nitrogen adsorption-desorption isotherms at 77 K and (b) pore-width distribution of rGO and rPGO composites.

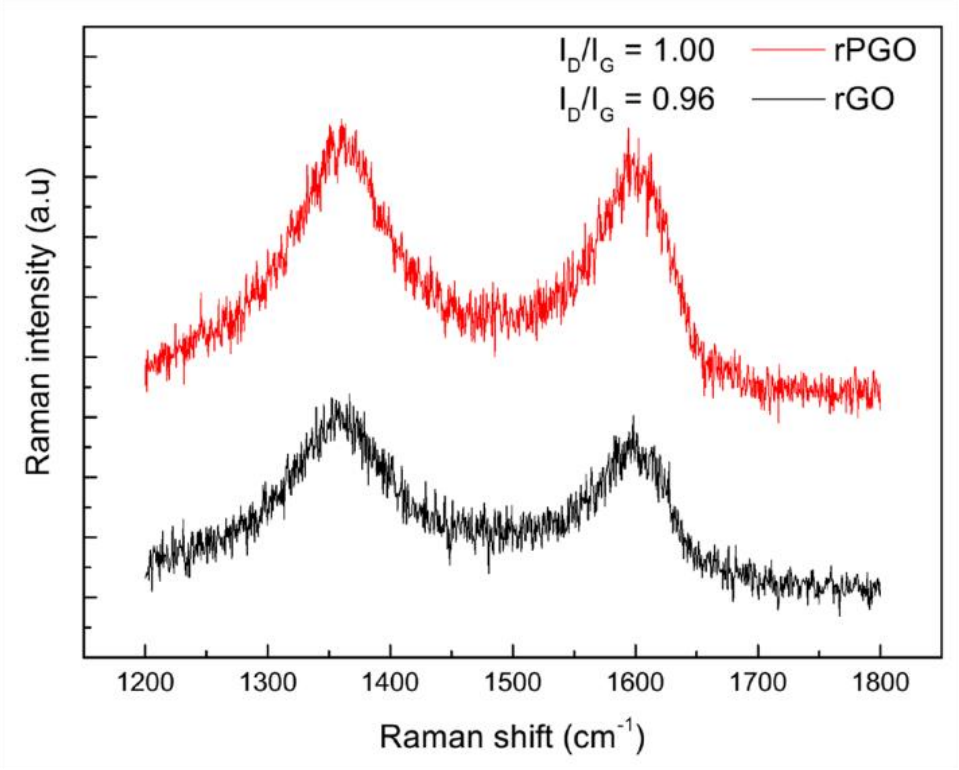

Figure 9 Raman spectra of rGO and rPGO in samples.

3.2 Electrochemical characterization

The electrochemical performances of the samples when used as anode materials were examined using a 2016 half-cell in the potential range of 0.01–3.0 V vs. Li^+/Li. Figure 10b-c show cyclic voltammetry (CV) curves for the first three cycles of MoS_2/rGO and MoS_2/rPGO electrode at a sweep rate of 0.5 mVs^{-1}. During the initial discharge (lithiation process), MoS_2/rPGO sample shows reduction peaks at ~ 0.8 V corresponding to lithiation of MoS_2 ($MoS_2 + xLi^+ + xe^{-1} \rightarrow Li_XMoS_2$), the formation of a gel-like polymeric layer and decomposition reaction of lithiated MoS_2 ($Li_xMoS_2 + (4-x)Li^+ + (4-x)e^- \rightarrow Mo + Li_2S$).[53] In the following reduction cycle, the peaks at ca. 1.3 V and 1.8 V are related to the lithiation process and the conversion reaction, respectively.[11, 27, 54, 55] These broad doublet peaks might be related to lithium intercalation reactions at different defect sites of disordered MoS_2, which is in accordance with XRD and TEM data indicating disordered phase of MoS_2.[20, 56, 57] In contrast to cycles of MoS_2 nanoparticle electrode illustrated in Figure 10a, 2nd and 3rd reduction cycle of MoS_2/rGO and MoS_2/rPGO electrode show overlapping peaks that suggest improved reversibility of MoS_2 due to conductivity compensation resulting from PGO and GO sheets.[53] Upon oxidation process, peaks ~ 1.9 V and ~ 2.3 V were observed and corresponded to delithiation process ($Li_2S \rightarrow S + 2Li^+$) and conversion reaction of Mo to MoS_2 ($Mo + Li_2S \rightarrow MoS_2$).[53, 58-61] Following 2nd and 3rd oxidation cycle also show good retention, which was similar to the behavior of the reduction cycles. The CV curves of MoS_2/rGO electrode show a similar behavior to that of the MoS_2/rPGO electrode (Figure 10c) while the MoS_2 nanoparticle electrode exhibited severe irreversibility of CV curves after cycling (Figure 10a). Figure 10e-f show the charge/discharge curves of MoS_2/rGO and MoS_2/rPGO electrodes, respectively, at a current density of 200 mA g^{-1}. Both the electrodes exhibit similar behavior of first three charge/discharge cycles. Broad potential plateaus up to 0.8 V during 1st lithiation process on MoS_2/rPGO electrode, and at around 1.5 V in the following discharge process are observed. During charge process, potential plateaus at around 1.8 V and 2.2 V corresponding to the conversion of Li_2S and Li_2S_x to sulfur are observed.[55, 62] All the charge/discharge curves are consistent with the results from the CV.

Electrochemical impedance spectroscopy (EIS) was performed to investigate improved electrochemical properties of MoS_2/rPGO sample (Figure 11). EIS was conducted at room temperature before and after 5 cycles at current density of 1 A g^{-1}. Nyquist plots of samples shown in Figure 11 exhibit semicircles in the medium-frequency range, which correspond to the charge transfer resistance of electrode.[35, 46] Both before and after 5 cycle, MoS_2/rPGO had lower charge transfer resistance than MoS_2/rGO, which suggesting enhancement of electrochemical properties of MoS_2/rPGO composite.

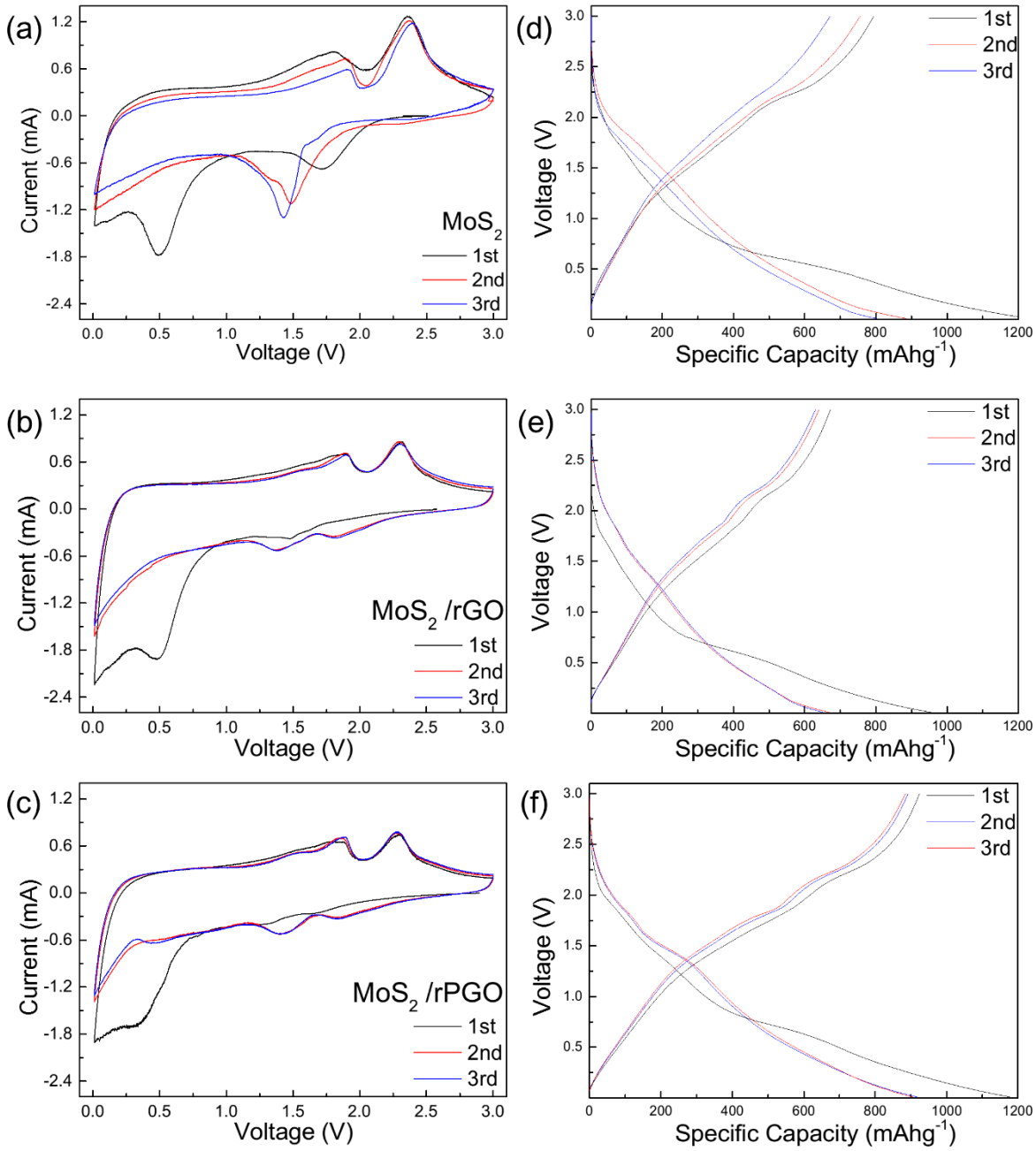

Figure 10 CVs of (a) MoS_2 nanoparticles, (b) MoS_2/rGO and (c) MoS_2/rPGO electrode for first to third cycles at a scan rate of 0.5 mV s^{-1}. First charge/discharge profiles of (d) MoS_2 nanoparticles and (e) MoS_2/rGO and (f) MoS_2/rPGO electrode at a current density of 200 mA g^{-1}.

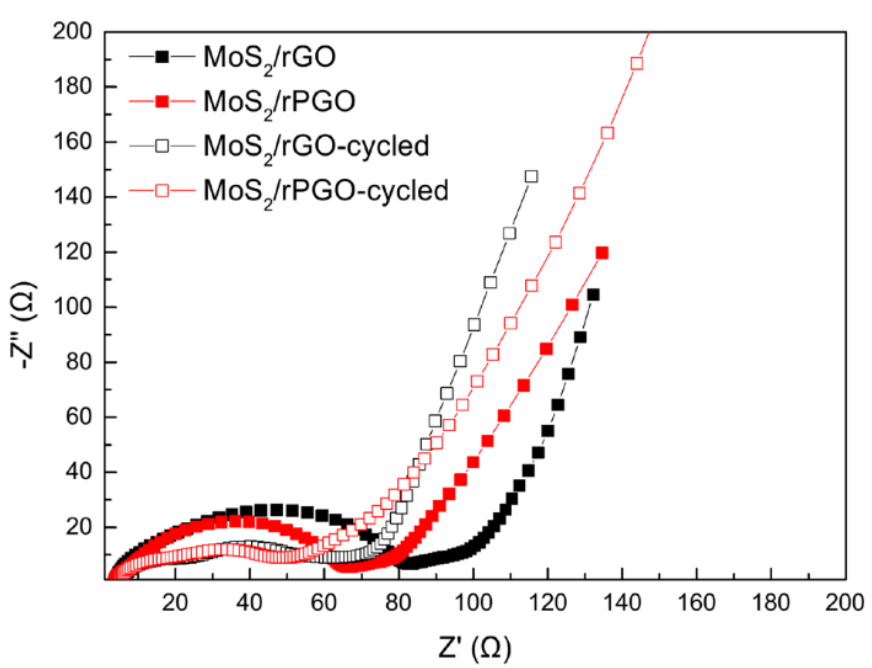

Figure 11 Nyquist plots of MoS_2/rGO and MoS_2/rPGO, before and after 5 cycles at 1 A g^{-1}.

Figure 12 exhibits the cycling behavior of MoS_2 nanoparticles, MoS_2/rGO and MoS_2/rPGO electrodes tested at a current density of 200 mA g^{-1}. The charge capacity of MoS_2 nanoparticles was 706 mA h g^{-1} during the first cycle and faded rapidly to 200 mA h g^{-1} after 100 cycles. In contrast, the MoS_2/rGO and MoS_2/rPGO electrode exhibited improved cyclic stability. Especially, the MoS_2/rPGO electrode exhibited an initial capacity of 924 mA h g^{-1} and 932 mA h g^{-1} after 100 cycles while capacity of the MoS_2/rGO electrode decreased from 672 to 395 mA h g^{-1}. The capacity improvement of the MoS_2/rPGO electrode compared to the MoS_2/rGO electrode could be due to increased surface area caused by the increased porosity in rPGO, which allows the composite accommodate more Li ions. The improved cyclic stability of the MoS_2/rPGO electrode might be attributed to its porous structure, which prevents restacking and condensation between sheets.[32, 63] Figure 12b exhibits the rate performance of MoS_2 nanoparticles examined at various current densities. At current densities of 100, 500, 2000 mA g^{-1}, the MoS_2/rPGO electrode has capacities of 1018, 787 and 451 mA h g^{-1}, respectively; the MoS_2/rGO electrode has capacities of 633, 478 and 292 mA h g^{-1}. The MoS_2 nanoparticle electrode shows a rapid capacity fading with increase in the current density, whereas the MoS_2/rPGO electrode retain their capacities. These improvement of capacity and rate properties might be also attributed to the enlarged surface area and pore volume caused by porous structure of rPGO.[31]

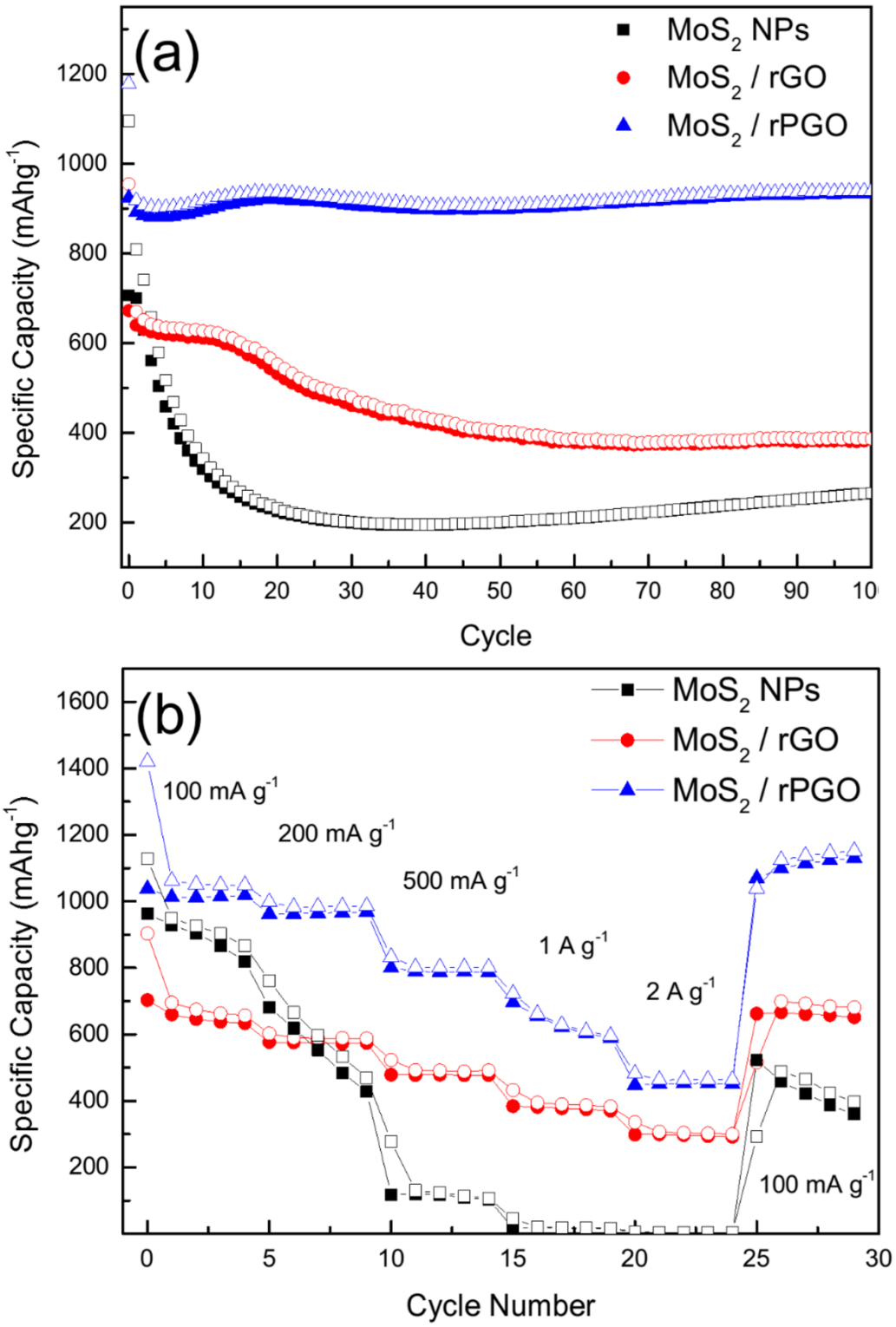

Figure 12 (a) Cycling performance at a current density of 200 mA g^{-1} and (b) rate capability performance of MoS_2 nanoparticles, MoS_2/rGO, MoS_2/rPGO.

For further investigation, we tested rPGO treated with ntric acid (4 M, 8 M and 12 M) as a substrate for preparation of rPGO/MoS_2 composites. Figure 13 shows rate capability performance of these samples. 4 M, 8 M and 12 M rPGO/MoS_2 composite exhibited capacity of 736, 1037 and 821 mA h g^{-1} at current density of 200 mA h g^{-1}, respectively. We therefore choose 8 M rPGO/MoS_2 composite as a representative material for this research on the basis of results depicted in Figure 13a. We also tested MoS_2/rPGO composite having different contents of MoS_2 and results of the samples are depicted in Figure 13b. We synthesized samples using 130, 150 and 170 g of $(NH_4)_2MoS_4$ as a precursor for MoS_2/rPGO composites and these samples showed 132, 451 and 280 mA h g^{-1} at current density of 2 A h g^{-1}. This means that proper amount of precursor is needed for better performance of composite.

Compared to previously published works for preparing the porous graphene-based composite anode materials, nitric acid treatment is inexpensive, simple and scalable to produce porous graphene oxide and PGO-based composite. The MoS_2 / nitric acid treated porous graphene oxide composite exhibited increased Li ion storage capacity and cycling stability owing to pores in grahpene oxide sheets. These pores provide additional edges and increase accessible surface area to accommodate Li ions.[64, 65] The enhancement of the electrochemical properties also can be attributed to the fact that the porous structure of rPGO prevents its composite from agglomeration by combining innate benefits of graphene and porous structure.[66, 67]

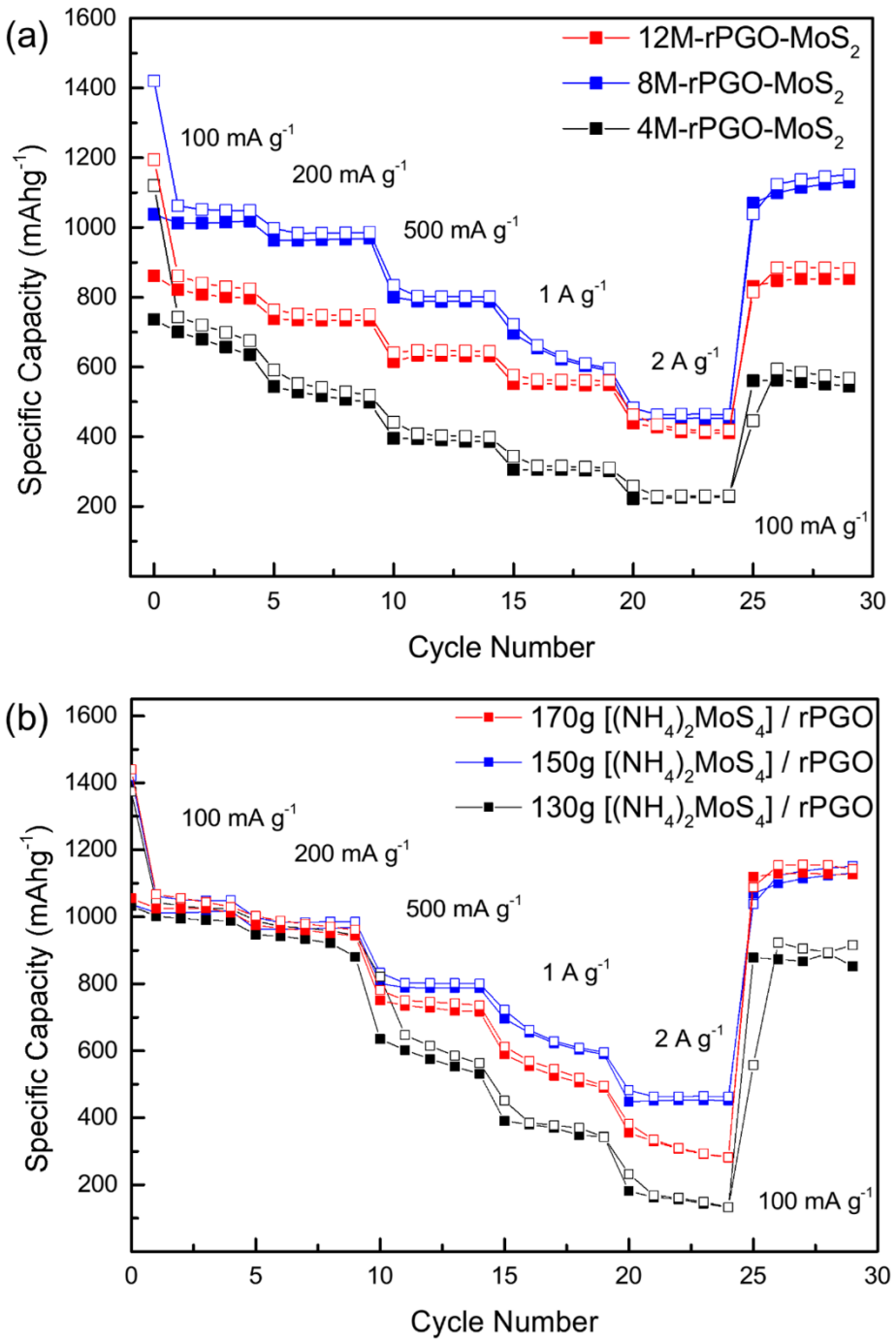

Figure 13 Rate capability performance of MoS_2/rPGO composite, a) synthesized using 12M, 8M and 4M nitric acid treat PGO as a substrate and b) synthesized using 130, 150 and 170g of $(NH_4)_2MoS_4$ as a precursor.

4. Conclusion

In summary, by using $(NH_4)_2MoS_4$ and PGO as precursors, MoS_2/rPGO nanocomposite was prepared by a simpFIGle solvothermal method. The PGO used here was synthesized by a simple and scalable nitric acid treatment precess. Pores in the rPGO sheets provide more active site for Li^+ storage and prevent aggregation of composites by reducing van der Waals interaction between sheets due to porous structure, which resulting improved electrochemical properties. BET analysis revealed that surface area and pore volume of MoS_2/rPGO are about 92.26 $m^2\ g^{-1}$ and 0.40 $cm^3\ g^{-1}$, which is larger than that of MoS_2/rGO. Compare to MoS_2/rGO and MoS_2 nanoparticle electrode, MoS_2/rPGO electrode possesses enhanced Li storage properties with a capacity of 923 mA h g^{-1} at current density of 200 mA g^{-1} after 100 cycles and 451 mA h g^{-1} at current density of 2 A g^{-1}. Our strategy has potential for practical applications, as it is cost-effective and simple.

References

[1] Z. Yang, J. Zhang, M.C.W. Kintner-Meyer, X. Lu, D. Choi, J.P. Lemmon, J. Liu, Electrochemical Energy Storage for Green Grid, Chemical Reviews, 111 (2011) 3577-3613.

[2] A. Manthiram, Y. Fu, S.-H. Chung, C. Zu, Y.-S. Su, Rechargeable Lithium–Sulfur Batteries, Chemical Reviews, 114 (2014) 11751-11787.

[3] M.S. Whittingham, Lithium Batteries and Cathode Materials, Chemical Reviews, 104 (2004) 4271-4302.

[4] M. Ge, J. Rong, X. Fang, C. Zhou, Porous Doped Silicon Nanowires for Lithium Ion Battery Anode with Long Cycle Life, Nano Letters, 12 (2012) 2318-2323.

[5] P. He, H. Yu, D. Li, H. Zhou, Layered lithium transition metal oxide cathodes towards high energy lithium-ion batteries, Journal of Materials Chemistry, 22 (2012) 3680-3695.

[6] P. Poizot, S. Laruelle, S. Grugeon, L. Dupont, J.M. Tarascon, Nano-sized transition-metal oxides as negative-electrode materials for lithium-ion batteries, Nature, 407 (2000) 496-499.

[7] C.-H. Lai, M.-Y. Lu, L.-J. Chen, Metal sulfide nanostructures: synthesis, properties and applications in energy conversion and storage, Journal of Materials Chemistry, 22 (2012) 19-30.

[8] K. Chang, D. Geng, X. Li, J. Yang, Y. Tang, M. Cai, R. Li, X. Sun, Ultrathin MoS_2/Nitrogen-Doped Graphene Nanosheets with Highly Reversible Lithium Storage, Advanced Energy Materials, 3 (2013) 839-844.

[9] Y. Xie, C. Wu, Design of nanoarchitectured electrode materials applied in new-generation rechargeable lithium ion batteries, Dalton Transactions, (2007) 5235-5240.

[10] Y. Wang, H. Li, P. He, E. Hosono, H. Zhou, Nano active materials for lithium-ion batteries, Nanoscale, 2 (2010) 1294-1305.

[11] T. Stephenson, Z. Li, B. Olsen, D. Mitlin, Lithium ion battery applications of molybdenum disulfide (MoS_2) nanocomposites, Energy & Environmental Science, 7 (2014) 209-231.

[12] A.B. Laursen, S. Kegnaes, S. Dahl, I. Chorkendorff, Molybdenum sulfides-efficient and viable materials for electro - and photoelectrocatalytic hydrogen evolution, Energy & Environmental Science, 5 (2012) 5577-5591.

[13] D. Kong, H. He, Q. Song, B. Wang, W. Lv, Q.-H. Yang, L. Zhi, Rational design of MoS_2@graphene nanocables: towards high performance electrode materials for lithium ion batteries, Energy & Environmental Science, 7 (2014) 3320-3325.

[14] J. Wang, J. Liu, D. Chao, J. Yan, J. Lin, Z.X. Shen, Self-Assembly of Honeycomb-like MoS_2 Nanoarchitectures Anchored into Graphene Foam for Enhanced Lithium-Ion Storage, Advanced Materials, 26 (2014) 7162-7169.

[15] Z. Wan, J. Shao, J. Yun, H. Zheng, T. Gao, M. Shen, Q. Qu, H. Zheng, Core–Shell Structure of Hierarchical Quasi-Hollow MoS_2 Microspheres Encapsulated Porous Carbon as Stable Anode for Li-Ion Batteries, Small, 10 (2014) 4975-4981.

[16] S. Ding, J.S. Chen, X.W. Lou, Glucose-Assisted Growth of MoS_2 Nanosheets on CNT Backbone for Improved Lithium Storage Properties, Chemistry – A European Journal, 17 (2011) 13142-13145.

[17] C. Wang, W. Wan, Y. Huang, J. Chen, H.H. Zhou, X.X. Zhang, Hierarchical MoS_2 nanosheet/active carbon fiber cloth as a binder-free and free-standing anode for lithium-ion batteries, Nanoscale, 6 (2014) 5351-5358.

[18] Z. Wang, T. Chen, W. Chen, K. Chang, L. Ma, G. Huang, D. Chen, J.Y. Lee, CTAB-assisted synthesis of single-layer MoS_2-graphene composites as anode materials of Li-ion batteries, Journal of Materials Chemistry A, 1 (2013) 2202-2210.

[19] C. Cui, X. Li, Z. Hu, J. Xu, H. Liu, J. Ma, Growth of MoS_2@C nanobowls as a lithium-ion battery anode material, RSC Advances, 5 (2015) 92506-92514.

[20] K. Chang, W. Chen, In situ synthesis of MoS_2/graphene nanosheet composites with extraordinarily high electrochemical performance for lithium ion batteries, Chemical Communications, 47 (2011) 4252-4254.

[21] Y. Gong, S. Yang, L. Zhan, L. Ma, R. Vajtai, P.M. Ajayan, A Bottom-Up Approach to Build 3D Architectures from Nanosheets for Superior Lithium Storage, Advanced Functional Materials, 24 (2014) 125-130.

[22] H. Jiang, D. Ren, H. Wang, Y. Hu, S. Guo, H. Yuan, P. Hu, L. Zhang, C. Li, 2D Monolayer MoS_2–Carbon Interoverlapped Superstructure: Engineering Ideal Atomic Interface for Lithium Ion Storage, Advanced Materials, 27 (2015) 3687-3695.

[23] K. Bindumadhavan, S.K. Srivastava, S. Mahanty, MoS_2-MWCNT hybrids as a superior anode in lithium-ion batteries, Chemical Communications, 49 (2013) 1823-1825.

[24] Y. Shi, Y. Wang, J.I. Wong, A.Y.S. Tan, C.-L. Hsu, L.-J. Li, Y.-C. Lu, H.Y. Yang, Self-assembly of hierarchical MoS_x/CNT nanocomposites ($2<x<3$) : towards high performance anode materials for lithium ion batteries, Scientific Reports, 3 (2013) 2169.

[25] L. Yang, S. Wang, J. Mao, J. Deng, Q. Gao, Y. Tang, O.G. Schmidt, Hierarchical MoS_2/Polyaniline Nanowires with Excellent Electrochemical Performance for Lithium-Ion Batteries, Advanced Materials, 25 (2013) 1180-1184.

[26] S. Stankovich, D.A. Dikin, G.H.B. Dommett, K.M. Kohlhaas, E.J. Zimney, E.A. Stach, R.D. Piner, S.T. Nguyen, R.S. Ruoff, Graphene-based composite materials, Nature, 442 (2006) 282-286.

[27] C. Zhu, X. Mu, P.A. van Aken, J. Maier, Y. Yu, Fast Li Storage in MoS_2-Graphene-Carbon Nanotube Nanocomposites: Advantageous Functional Integration of 0D, 1D, and 2D Nanostructures, Advanced Energy Materials, 5 (2015) 1401170.

[28] X. Zhou, L.-J. Wan, Y.-G. Guo, Facile synthesis of MoS_2@CMK-3 nanocomposite as an improved anode material for lithium-ion batteries, Nanoscale, 4 (2012) 5868-5871.

[29] L. Jiang, Z. Fan, Design of advanced porous graphene materials: from graphene nanomesh to 3D architectures, Nanoscale, 6 (2014) 1922-1945.

[30] C. Uthaisar, V. Barone, Edge Effects on the Characteristics of Li Diffusion in Graphene, Nano Letters, 10 (2010) 2838-2842.

[31] Z. Fan, J. Yan, G. Ning, T. Wei, L. Zhi, F. Wei, Porous graphene networks as high performance anode materials for lithium ion batteries, Carbon, 60 (2013) 558-561.

[32] Z. Jiang, B. Pei, A. Manthiram, Randomly stacked holey graphene anodes for lithium ion batteries with enhanced electrochemical performance, Journal of Materials Chemistry A, 1 (2013) 7775-7781.

[33] D. Pan, S. Wang, B. Zhao, M. Wu, H. Zhang, Y. Wang, Z. Jiao, Li Storage Properties of Disordered Graphene Nanosheets, Chemistry of Materials, 21 (2009) 3136-3142.

[34] Z.-L. Wang, D. Xu, H.-G. Wang, Z. Wu, X.-B. Zhang, In Situ Fabrication of Porous Graphene Electrodes for High-Performance Energy Storage, ACS nano, 7 (2013) 2422-2430.

[35] L. Liao, J. Zhu, X. Bian, L. Zhu, M.D. Scanlon, H.H. Girault, B. Liu, MoS2 Formed on Mesoporous Graphene as a Highly Active Catalyst for Hydrogen Evolution, Advanced Functional Materials, 23 (2013) 5326-5333.

[36] X. Huang, K. Qian, J. Yang, J. Zhang, L. Li, C. Yu, D. Zhao, Functional Nanoporous Graphene Foams with Controlled Pore Sizes, Advanced Materials, 24 (2012) 4419-4423.

[37] B.G. Choi, M. Yang, W.H. Hong, J.W. Choi, Y.S. Huh, 3D Macroporous Graphene Frameworks for Supercapacitors with High Energy and Power Densities, ACS nano, 6 (2012) 4020-4028.

[38] Y. Xu, K. Sheng, C. Li, G. Shi, Self-Assembled Graphene Hydrogel via a One-Step Hydrothermal Process, ACS nano, 4 (2010) 4324-4330.

[39] X. Wang, L. Jiao, K. Sheng, C. Li, L. Dai, G. Shi, Solution-processable graphene nanomeshes with controlled pore structures, Scientific Reports, 3 (2013) 1996.

[40] D. Xie, W.J. Tang, X.H. Xia, D.H. Wang, D. Zhou, F. Shi, X.L. Wang, C.D. Gu, J.P. Tu, Integrated 3D porous C-MoS_2/nitrogen-doped graphene electrode for high capacity and prolonged stability lithium storage, Journal of Power Sources, 296 (2015) 392-399.

[41] R. Wang, C. Xu, J. Sun, Y. Liu, L. Gao, H. Yao, C. Lin, Heat-induced formation of porous and free-standing MoS_2/GS hybrid electrodes for binder-free and ultralong-life lithium ion batteries, Nano Energy, 8 (2014) 183-195.

[42] N. Lingappan, D.J. Kang, Molybdenum Disulfide Nanosheets Interconnected Nitrogen-Doped Reduced Graphene Oxide Hydrogel: A High-Performance Heterostructure for Lithium-Ion Batteries, Electrochimica Acta, 193 (2016) 128-136.

[43] W.S. Hummers, R.E. Offeman, Preparation of Graphitic Oxide, Journal of the American Chemical Society, 80 (1958) 1339-1339.

[44] Y. Li, H. Wang, L. Xie, Y. Liang, G. Hong, H. Dai, MoS_2 Nanoparticles Grown on Graphene: An Advanced Catalyst for the Hydrogen Evolution Reaction, Journal of the American Chemical Society, 133 (2011) 7296-7299.

[45] C. Zhao, J. Kong, X. Yao, X. Tang, Y. Dong, S.L. Phua, X. Lu, Thin MoS_2 Nanoflakes Encapsulated in Carbon Nanofibers as High-Performance Anodes for Lithium-Ion Batteries, ACS Applied Materials & Interfaces, 6 (2014) 6392-6398.

[46] X. Zheng, J. Xu, K. Yan, H. Wang, Z. Wang, S. Yang, Space-Confined Growth of MoS_2 Nanosheets within Graphite: The Layered Hybrid of MoS_2 and Graphene as an Active Catalyst for Hydrogen Evolution Reaction, Chemistry of Materials, 26 (2014) 2344-2353.

[47] K.S. Liang, R.R. Chianelli, F.Z. Chien, S.C. Moss, Structure of poorly crystalline MoS_2 — A modeling study, Journal of Non-Crystalline Solids, 79 (1986) 251-273.

[48] H.W. WANG, P. SKELDON, G.E. THOMPSON, G.C. WOOD, Synthesis and characterization of molybdenum disulphide formed from ammonium tetrathiomolybdate, Journal of Materials Science, 32 (1997) 497-502.

[49] A. Lerf, H. He, M. Forster, J. Klinowski, Structure of Graphite Oxide Revisited, The Journal of Physical Chemistry B, 102 (1998) 4477-4482.

[50] S. Stankovich, D.A. Dikin, R.D. Piner, K.A. Kohlhaas, A. Kleinhammes, Y. Jia, Y. Wu, S.T. Nguyen, R.S. Ruoff, Synthesis of graphene-based nanosheets via chemical reduction of exfoliated graphite oxide, Carbon, 45 (2007) 1558-1565.

[51] J. Yan, T. Wei, B. Shao, Z. Fan, W. Qian, M. Zhang, F. Wei, Preparation of a graphene nanosheet/polyaniline composite with high specific capacitance, Carbon, 48 (2010) 487-493.

[52] J. Yan, Y. Xiao, G. Ning, T. Wei, Z. Fan, Facile and rapid synthesis of highly crumpled graphene sheets as high-performance electrodes for supercapacitors, RSC Advances, 3 (2013) 2566-2571.
[53] K. Chang, W. Chen, l-Cysteine-Assisted Synthesis of Layered MoS_2/Graphene Composites with Excellent Electrochemical Performances for Lithium Ion Batteries, ACS nano, 5 (2011) 4720-4728.
[54] X. Cao, Y. Shi, W. Shi, X. Rui, Q. Yan, J. Kong, H. Zhang, Preparation of MoS_2-Coated Three-Dimensional Graphene Networks for High-Performance Anode Material in Lithium-Ion Batteries, Small, 9 (2013) 3433-3438.
[55] X. Fang, C. Hua, X. Guo, Y. Hu, Z. Wang, X. Gao, F. Wu, J. Wang, L. Chen, Lithium storage in commercial MoS_2 in different potential ranges, Electrochimica Acta, 81 (2012) 155-160.
[56] X. Fang, X. Yu, S. Liao, Y. Shi, Y.-S. Hu, Z. Wang, G.D. Stucky, L. Chen, Lithium storage performance in ordered mesoporous MoS2 electrode material, Microporous and Mesoporous Materials, 151 (2012) 418-423.
[57] G. Wang, S. Bewlay, J. Yao, H. Liu, S. Dou, Tungsten disulfide nanotubes for lithium storage, Electrochemical and solid-state letters, 7 (2004) A321-A323.
[58] G. Du, Z. Guo, S. Wang, R. Zeng, Z. Chen, H. Liu, Superior stability and high capacity of restacked molybdenum disulfide as anode material for lithium ion batteries, Chemical Communications, 46 (2010) 1106-1108.
[59] H. Liu, D. Su, R. Zhou, B. Sun, G. Wang, S.Z. Qiao, Highly Ordered Mesoporous MoS_2 with Expanded Spacing of the (002) Crystal Plane for Ultrafast Lithium Ion Storage, Advanced Energy Materials, 2 (2012) 970-975.
[60] B. Luo, Y. Fang, B. Wang, J. Zhou, H. Song, L. Zhi, Two dimensional graphene-SnS_2 hybrids with superior rate capability for lithium ion storage, Energy & Environmental Science, 5 (2012) 5226-5230.
[61] B. Scrosati, J. Hassoun, Y.-K. Sun, Lithium-ion batteries. A look into the future, Energy & Environmental Science, 4 (2011) 3287-3295.
[62] F. Pan, J. Wang, Z. Yang, L. Gu, Y. Yu, MoS_2-graphene nanosheet-CNT hybrids with excellent electrochemical performances for lithium-ion batteries, RSC Advances, 5 (2015) 77518-77526.
[63] X. Zhao, C.M. Hayner, M.C. Kung, H.H. Kung, Flexible Holey Graphene Paper Electrodes with Enhanced Rate Capability for Energy Storage Applications, ACS nano, 5 (2011) 8739-8749.
[64] C. Menachem, E. Peled, L. Burstein, Y. Rosenberg, Characterization of modified NG7 graphite as an improved anode for lithium-ion batteries, Journal of Power Sources, 68 (1997) 277-282.
[65] M. Winter, J.O. Besenhard, M.E. Spahr, P. Novák, Insertion Electrode Materials for Rechargeable Lithium Batteries, Advanced Materials, 10 (1998) 725-763.

[66] S. Han, D. Wu, S. Li, F. Zhang, X. Feng, Porous Graphene Materials for Advanced Electrochemical Energy Storage and Conversion Devices, Advanced Materials, 26 (2014) 849-864.
[67] Y. Lin, X. Han, C.J. Campbell, J.-W. Kim, B. Zhao, W. Luo, J. Dai, L. Hu, J.W. Connell, Holey Graphene Nanomanufacturing: Structure, Composition, and Electrochemical Properties, Advanced Functional Materials, 25 (2015) 2920-2927.

국문초록

리튬 이온 배터리는 휴대용 전자기기와 하이브리드 자동차등 다양한 전자기기에 전원을 공급하는 장치로 널리 사용되고 있다. 최근 전자기기들이 고도화됨에 따라 높은 에너지 밀도와 고출력의 리튬 이온 배터리에 대한 요구가 증가하고 있다. 이러한 수요를 충족시키기 위해 높은 정전 용량을 갖는 전극 물질들이 연구되고 있다. 다양한 전극 물질 중, 이황화 몰리브덴(MoS_2) 은 한 개의 MoS_2 분자에 4 개의 리튬 이온이 삽입되는 반응을 통해 기존의 흑연 전극의 정전 용량 (372 mA h g^{-1}) 보다 높은 정전 용량을 (670 mA h g^{-1}) 보여 기존의 흑연을 대체할 후보 물질으로 주목 받고 있다. 그러나 MoS_2 의 낮은 전기/ 이온 전도도로 인해 리튬 저장 용량과 충방전 특성이 저하되는 현상이 발생한다. 본 학위 논문에서는 용매열 합성법을 이용해 MoS_2 와 환원 다공성 그래핀 옥사이드(rPGO) 복합체를 형성하였다. 그를 통해 MoS_2 의 전도도를 보완하여 리튬 저장 특성을 증가시키려 하였다. 다공성 그래핀 옥사이드는 그래핀 옥사이드를 에칭하여 기공구조를 부여한 것으로 고유의 기공 구조로 인해 시편의 재적층 현상을 감소시키고 리튬 이온의 이동 통로를 제공하여 리튬 이온 저장 성능을 개선시킬 수 있다. 다공성 그래핀 옥사이드는 쉽고 편하며 대량 생산이 가능한 질산 처리법을 이용해 제조하였다. 넓어진 표면적과 다공성 구조로 인해, MoS_2/ rPGO 시편은 MoS_2/ 환원 그래핀 옥사이드(rGO) 시편에 비해 향상된 충전 용량과 내구성을 보여주었다. 충·방전이 100 회 진행되었을 때, MoS_2/ rGO 전극은

200 mA g^{-1}의 충전 속도에서 395 mA h g^{-1}의 충전 용량을 나타낸 반면 MoS_2/rPGO 전극은 같은 충전 속도에서 932 mA h g^{-1}의 충전 용량을 나타내었다. 이는 다공성 그래핀 옥사이드의 기공 구조가 적층 현상을 방지하고 리튬 이온의 원활한 이동을 도와 MoS_2의 리튬 이온 저장 특성을 효과적으로 개선하는 것을 보여준다.

주요어 : 리튬이온전지, 음극, 다공성 산화 그래핀, 이황화 몰리브덴, 탄소 복합체

학 번: 2015-26026